I x-mg-wavelength stacked $Si_{1-x}Ge_x$/Si heterojunction internal photoemission in frared detectors

J. S. Park, T. L. Lin, E. W. Jones, H. M. Del Castillo, T. George and S. D. Gunapala

Center for Space Microelectronics Technology, Jet Propulsion Laborato y
California Institute of Technology, 4800 Oak Grove Dr., Pasadena, CA 9 109

ABSTRACT

Utilizing the low temperature silicon molecular beam epitaxy (M BE) growth of degenerately doped SiGe la ycrs on Si, long wavelength stacked SiGe/Si heterojunct ion internal photoemission (111P) infrared detectors with multiple SiGe/Si layers have been fabricated and demonstrated. The detector structure consists of several periods of degenerately boron doped thin ($\leq$ 50 Å) SiGe layers and undoped thick ($\approx$ 300 Å) Si layers. The stacked SiGe HIP detectors arc expected to exhibit higher quantum efficiencies than single layer HIP detectors due to thin SiGe layers which can enhance the internal quantum efficiency. Using elemental boron as a dopant source during the low temperature MBE growth, high doping concentration ($\approx 4 \times 10^{20}$ cm^{-3}) has been achieved and high crystalline quality multiple SiGe/Si layers have been obtained. For the. experiment several stacked $Si_{0.7}Ge_{0.3}$/Si HIP detectors with various SiGe layer thickness and doping concentration have been fabricated. The detectors have exhibited strong infrared absorption and near ideal thcrmionic-emission dark current characteristics. For the stacked $Si_{0.7}Ge_{0.3}$/Si HIP detectors with [B] = 4×10^{20} cm^{-3}, strong photoresponse at wavelengths ranging 2 to 20 pm has been measured. Enhanced quantum efficiencies, especially in the long wavelength regime ($\lambda > 10$ pm), have been observed compared to those of our single layer SiGe HIP detectors with the same Ge concentration, doping concentration and total SiGe layer thickness, which is due to the enhanced internal quantum efficiency. The effects of doping concentration on the detector optical and electrical characteristics have been studied, Using the measured quantum efficiency and dark current data, detectivity ($D\lambda^*$) of detectors has been estimate.d.

1. INTRODUCTION

1 ong wavelength infrared (LWIR) detector focal plane arrays operating in the range of 8 to 17 μm have been of great interest for a variety of space and defense applications. Recently, with the advent of the silicon molecular beam epitaxy (Si-Mill{) growth technique, novel SiGe/Si heterojunction internal photoemission (I 111') IR detectors have been fabricated and demonstrated to exhibit tailorable detector response in the long wavelength infrared regime.[1-5] The SiGe/Si I 111' detectors can be easily integrated

with Si readout circuitry either monolithically or by iridium bump bonding, and are expected to exhibit excellent pixel-to-pixel uniformity and good device reliability. Recently, using SiGe/Si HIP detector elements and monolithic CCD readout circuitry, 400 x 400 focal plane arrays with 10 μm cut-off wavelength were fabricated by Tsaur *et. al*, and high quality images were demonstrated.[4,5]

The idea of the heterojunction internal photoemission (1111') detector was first proposed by Shepherd *et. al* in 1971.6 However, due to the lack of epitaxial layer growth technology, the concept was not implemented until 1990 when Lin *et . al* first demonstrated SiGe/Si HIP detectors using an advanced Si-MBE growth technique. [1] The SiGe/Si HIP detector consists of a degenerately doped p^+-SiGe layer as an emitter and a p-type. Si substrate as a collector. The device structure and band diagram are shown in Fig. 1 (a) and (b), respectively. The detection mechanism involves strong infrared absorption in the p^+-SiGe emitter layer mainly through free carrier absorption followed by the internal photoemission of photo-excited holes over the SiGe/Si heterojunction barrier into the Si substrate, as shown in Fig. 1(b). The cutoff wavelength λ_c of the HIP detector is determined by the effective barrier height $q\Phi_b$, and is given by

$$\lambda_c(\mu m) = 1.24/q\Phi_b\,(eV) \qquad \textbf{(I).}$$

The effective barrier $q\Phi_b$ is determined by the valence band offset (ΔE_V) between Si 1-xGex layer and Si substrate, and the Vcmli-level E_f in the SiGe layer, alit] is given by

$$q\Phi_b = \Delta E_V - (E_V - E_f) \qquad (2).$$

The valence band offset ΔE_V between strained Si 1-xGex and Si layers and the I 'ermi-level E_f can be tailored by changing the Ge composition and doping concentration in the SiGe layer, respectively. '1'bus, for SiGe/Si HIP IR detectors, by engineering the Ge and doping concentrations of Si 1-xGex layer, the cut-off wavelength can be tailored over a wide IR range (3-30 pm). The tailorable cut-off wavelength can be used to opt imize the trade-off between the LWIR response and the cooling requirement of the detector.

The external quantum efficiency (η) of an internal photoemission detector is a product of absorptance (A) in SiGe layers and internal quantum efficiency (η_i) which is defined as the ratio of the collected holes to the photo-excited holes (i.e., $\eta = A\,\eta_i$). SiGe/Si HIP detectors offer higher internal quantum efficiency than silicide Schottky barrier- detectors due to substantially smaller l;ermi-energy of pi -SiGe layers. [1,2,5] The internal quantum cffiCiCncy of 1111} detectors are limited by inelastic hole-hole and hole- phonon scatterings as well as the number of holes redirected rom the SiGe/air interface to the

SiGe/Si interface. Reducing the SiGe layer thickness enhances the internal quantum efficiency since photo-excited holes would suffer less inelastic scattering[8]; however, reducing the SiGe layer thickness reduces infrared absorption as well. "J'bus, the optimal SiGe layer thickness is determined by the trade-off between absorption and internal quantum efficiency. One way of achieving high internal quantum efficiency without losing absorption is by incorporating thin multiple absorbing SiGe layers which arc stacked between Si barriers. The detection mechanism of a stacked SiGe/Si HIP detector is schematically illust.rated in Fig. 2 and it is similar to that of single layer SiGe/Si HIP detectors. In this case, each individual layer has high η_i due to the thin SiGe layer and the absorption from each layer contributes to the total absorption. Furthermore, due to the applied electric field toward the Si substrate (z-direction), the photo-excited holes traveling opposite to' z-direction will be redirected toward the Si substrate. This wiii further increase the internal quantum efficiency.

2. MBE GROWTH OF STACKED SiGe/Si HIP DETECTORS

To gain high photoresponse, degenerate doping in the SiGe emitter layer with abrupt doping profiles and high quality epitaxial layers with smooth SiGe/Si hetero-interface arc essential. These requirements can be achieved by the MBE growth of SiGe layers at low temperatures using elemental boron source for doping. For a SiGe/Si heterostructure, the lattice mismatch between $Si_{1-x}Ge_x$ and Si layers induces strain in the $Si_{1-x}Ge_x$ layer. Due to this strain, a $Si_{1-x}Ge_x$ layer can be grown pseudomorphically only up to a small thickness which is called "critical thickness"[9]. Beyond the ci itical thickness, the $Si_{1-x}Ge_x$ layer will resume its natui al lattice constant by generating misfit dislocations at the hetero-interface. The growth of high a quality strained SiGe layer requires some key conditions, such as an ultra high vacuum, low growth temperature. and clean substrate surface. Among them, low growth temperature is the most critical condition. High temperature growth causes strain relaxation and allows three dimensional growth (island formation) of the SiGe layer which results in poor morphology. To obtain high crystalline quality strained $Si_{1-x}Ge_x$ layers, the growth temperature should be kept below 500 °C.[9]

Previously, for our SiGe/Si HIP detector structure growth, 1 HBO_2 was used as the boron dopant source for the p^+ SiGe layers growth. A 1 HBO_2 source has the advantage of exhibiting high vapor pressure that allows the usc of a conventional Knudsen cell to evaporate the required high dopant flux. [10] However, due to the doping mechanism in HBO_2, a relatively high growth temperature (>650 °C) is

required for high quality crystalline growth for the following, reactions: '1' > SO() °C for the initial reaction with Si to form elemental boron and silicon dioxide; T >650 °C for the removal of the incorporated oxygen by reaction of silicon dioxide with silicon to form volatile SiO. The use of HBO_2 at the low growth temper'aturc required for strained SiGe layer growth introduces a high level of oxygen contamination in SiGe layers and an incomplete reaction with Si to form elemental boron, Figures 4 (a) and (b) show the cross-sectional TEM micrographs of 25-nm-thick undoped and HBO_2 doped ($p^+ \approx 2 \times 10^{20}$ cm^{-3}) $Si_{0.7}Ge_{0.3}$ layers grown by MBE at 500 °C. The quality of the HBO_2 doped sample is significantly worse than that of the undoped sample, revealing very rough surface morphology and high defect density (2. x 1 0^{10} cm^{-2}) which is caused by low temperature growth.

The p^+-SiGe layer growth problems associated with HBO_2 source can be resolved by using elemental boron evaporated from a high-temperature Knudsen cell (due to the low vapor pressure of the elemental boron, high temperature, 1700- 1900 °C, evaporation is required. 3'bus, a speciall y designed Knudsen cell is required).[3] The elemental boron allows very sharp and high doping profiles with good crystalline quality epitaxial layers over a wide range of temperature (ewe.n below 400 °C). Figur c 4 shows a secondary ion mass spectroscopy (SIMS) doping profile using an elemental boron source after Ref. 11. The figure shows extremely sharp doping profiles revealing 10 periods of p' -Si/ p^--Si layers with decay length of about 20 Å. The usc of elemental boron enables us to grow high qualit y stacked SiGe/Si HIP detectors with multiple p^+-SiGe/p^--Si layers for which hyper sharp doping profiles and smooth hetero-interfaces are indispensable. Figure 5 shows a closs-sectional "1'1 :M micro graph of a MBE grown multiple p^+-SiGe/p^--Si layer structure. The growth temperature was 380 °C anti the elemental boron was used for the growth of p^+-SiGe layers with 4 x 10^{20} cm^{-3} doping concentration. It shows very smooth and flat interfaces between SiGe/Si and no defects within the TEM resolution. '1'bus, using the elemental boron source, high crystalline quality p^+-strained SiGe layers can be grown at low temperatur e which ensures strain conservation and smooth morphology.

The stacked layer SiGe/Si HIP detectors were fabricated by MBE growth of multiple p^+-$Si_{1-x}Ge_x$ and undoped-Si layers on oxide patterned p^--type Si(100) wafer's where rl-type guard rings were incorporated at the periphery of the active detector area to minimize. edge leakage current. Prior to MBE growth, a wafer was cleaned using the "spin-clean" method which involve. s the removal of a chemically grown protective oxide using an HF/ethanol solution in it nitrogen grove box.[12] Then, the wafer was loaded into a commercial Riber EVA 32 Si MBE system with a base pressure of 3 x 10-11 torr, and heated to 650 °C to remove the protective oxide. Ge and Si were evaporated from electron-gun sources, and elemental boron was evaporated from a high-temperature Knudsen cell. The growth temperatur e was maintained at 380 0,:. '1'hen, the detectors were fabricated by standard Si processing steps which included plasma etching of MBE grown SiGe/Si layers and aluminum evaporation/patterning to make ohmic contacts on the top pi -SiGe layer and boron implanted Si-p^+ wells as shown in Fig. 1 (a).

3. RESULTS AND DISCUSSION

The infrared absorption of the multiple SiGe/S i layers was characterized with a Fourier transform infrared (FTIR) spectrometer. Figure 6 shows the absorption spectrum of a multiple SiGe/Si layers which consists of four periods of 50 Å-thick p^+- $Si_{0.7}Ge_{0.3}$ layers and 300 Å-thick undoped Si layers. The SiGe layers were boron doped to about 4×10^{20} cm^{-3}. The absorption increases monotonically with wavelength, and strong absorption (30 to 45%) is obtained beyond 10 µm. The infrared absorption is mainly due to the strong free carrier absorption caused by the heavy doping in the SiGe layers, The small peak near 3 µm is due to the valence intraband transition. [1]3*14

The photoresponse of the stacked 1111' detectors was measured using a glow bar, a monochromator with several band pass filters to eliminate the higher order effects from gratings, and a pyroelectric detector to calibrate photon flux. Infrared illumination was applied on the front side of the detectors. Figure 7 shows the photoresponse spectra of a stacked 111P detector (detector A) in terms of external quantum efficiency. 'l'he detector consists of three 50 Å-thick p^+-$Si_{0.7}Ge_{0.3}$ layers which are separated by 300 Å-thick undoped Si layers. The Ge concentration and boron concentration are 30 % and 4 xl 0^{20} cm^{-3}, respectively. The active detector areas are 1.2.5 xl $()^{-3}$ cm^{-2}. The operating temperature and bias voltage are 30 K and -().5 V (positive to the top SiGe layer), respectively.

The detector shows broad photoresponse which cut off at around 20 pm. The peak response lies at around 5 µm with 6 % external quantum efficiency. The response gradually decreases as the wavelengt h increases and a small bump is observe.d near 14 µm. The detector manifests about 4 and 2 % external quantum efficiencies at 10 µm and 15 µm wavelengths, respective] y. This stacked SiGe/Si HIP detector, in general, exhibits higher quantum efficiency in the LWIR regime (λ>10µm) than our single layer SiGe/Si HIP detectors with the same Ge concentration, doping concentration and SiGe layer thickness. For example, a 200 Å-thick Sio.7Gco.#Sin HIP detector with p = 4 x 1020 cm~ showed quantum efficiencies of about 2 % at 10µm and less than 1% at 15 pm. 'J he enhancement of quantum efficiency can be due to the enhancement of internal quantum efficiency for the stacked SiGe/Si HIP detector, especially in the. long wavelength regime where photo-excited holes have small kinetic energies to cross over a potential barrier. l'bus, the results indicate that stacking thin SiGe layers is useful to enhance the internal quantum efficiency. Figure 8 shows the bias dependen t photoresponse of this stacked SiGe/Si HIP detector. The wavelength was fixed at 10 µm. With small bias (0 to 0.2 V), the quantum efficiency increases rapidly. While above 0.2 V bias it increases slowly, and finally it gets saturated above 1 V.

'l'he 1-V characteristics of the stacked SiGe/Si HIP detectors were measured at several temperatures. Forward and reverse bias modes show asymmetric I-V characteristics, because a larger leakage current occurs under forward bias. Fig.9 shows reverse-bias dark current characteristics of a stacked SiGe/Si HIP detector (detector B) with four 25 Å pi -$Si_{0.7}Ge_{0.3}$ layers separated by 300 Å undoped Si layers. This detector shows a similar photoresponse as shown in Fig. 7 with about 20 μm cut-off wavelength. The doping concentration for this detector is 4 x 10^{20} cm^{-3}. The effective barrier height can be estimated by activation energy analysis. [1,3] For the stacked SiGe/Si I 111' detectors, dark current is dominated by the thermionic-emission current, especially at low bias, which is given by

$$Jo=- A^{**} T^2 \exp(-\Phi_b/kT)$$

where A** is the Richardson constant, T is the absolute temperature, K is Boltzmann constant, and $q\Phi_b$ is effective barrier height. 'l'he above equation is derived for the three-dimensional thermionic-emission case, but the equation can still be applied to the present stacked SiGe/Si HIP detectors, in spite of possible subband formation inside SiGe layers due to the thin SiGe layers sandwiched between Si potential barriers. This is because subbands are occupied up to considerably high energy states due to large Fermi-level energ y (150 meV) in SiGe layers which is caused by dc.generate eloping. Figure 10 shows the *activation* energy plot for the stacked HIP detector shown in Fig.9 at -0.1 V bias. The effective barrier height determined from the linear slop is 60.4 meV which corresponds to 20.5 μm cut off wavelength; and A** determined from the ordinate intercept at 1/kT = 0 is 4.5 $A/cm^2/K^2$. This estimated barrier height agrees well with the observed cut-off wavelength shown in Fig. 7. The small A** values indicates that the epitaxial layer quality of multiple SiGe/Si layers is excellent, and the dark current is limited by the ideal thermionic-emi ssion current.

Stacked SiGe/Si HIP detectors for 5-10 μm application have also been fabricated using lower doping concentrations. Detectors C and D consist of three 50 Å-thick pi -$Si_{0.7}Ge_{0.3}$ layers which arc separated by 300 Å-thick undoped Si layers. Doping concentrations are about 1 x 102°" and 2x 1020 cm^{-3} for detectors C and D, respectively. Figure 11 shows external quantum efficiency vs. wavelength for detector C (open square) and detector D (filled square), Both detectors show peaks at around 5 μm with quantum efficiency of 3-4 %. The quantum efficiency drops rapidly with increasing wavelength. At around 10 pm, quantum efficiencies of 0.7 and 0.5 % arc measured for detector C and detector D, respectively. Detectors C anti D show the cut-off wavelengths of about 17 and 15 μm, respectively. These values are smaller than the cut-off wavelengths of detectors A and B. "l'his indicates that a detector with lower doping concentration exhibits shorter cut-off wavelength as was expected from Eq.

(2) due to smaller Ef. The reverse bias J-V characteristics of detector D at several temperatures is shown in Fig. 12 for comparison with those of detector A and B. It shows much smaller dark current than detector A and B. Consequently, this detector can be operated at higher temperatures.

The defectivity of the stacked 111P detectors can be estimated from the measured quantum efficiency and dark current. The D* is estimated by[15]

$$D_\lambda^* = QE \frac{1}{1.24} \sqrt{A} / i_n \ (cm\sqrt{Hz}/W) ,$$

where η is the external quantum efficiency, A is the detector area ant] λ is the wavelength (pm). i_n is the dark current noise which is given by

$$i_n = \sqrt{4qI_d \Delta f}$$

where I_d is the dark current, g is the photocurrent gain and Af is the bandwidth. Assuming a unity current gain (g = 1), wc have estimated $D\lambda^*$'s of the detectors at several temperatures and arc plotted in Fig. 13 for detector B and D. For both cases, the bias voltage is -0.2. V which gives relatively high quantum efficiency with low dark current. Detector B shows broad spectrum with $D\lambda^* > 1$ x1010 $cm\sqrt{Hz}/W$ at 40 K over 4-16 μm wavelength range; and detector D shows $D\lambda^* > 1x10^{10}$ $cm\sqrt{Hz}/W$ at 60 K over 3-9 μm wavelength range.

4. SUMMARY

in summary, we have demonstrated stacked SiGe/Si HIP infrared detectors using multiple $Si_{0.7}Ge_{0.3}$/Si layers, High crystalline quality multiple p^+-$Si_{0.7}Ge_{0.3}$/p^--Si layers were grown by low temperature MBE technique incorporating elemental boron source for doping. The detectors showed very strong infrared absorption and near ideal thermionic-emission limited dark current characteristics. The stacked $Si_{0.7}Ge_{0.3}$/Si 111P detector with $p = 4 \times 10^{20}$ cm^{-3} showed strong photoresponse at the wavelength between 2 to 20 μm with a external quantum efficiency of about 2 % at 15 μm. They showed enhanced quantum efficiencies, especially in the long wavelength regime, than our single layer SiGe/Si HIP detectors. This is ehnahcement is due to the enhanced internal quantum efficiency. Stacked $Si_{0.7}Ge_{0.3}$/Si HIP detectors with lower doping concentrations have been fabricated as well. They exhibited shorter cut-off wavelengths than the detectors with higher doping concentrations due to the smaller l;crmi-energy. Detectivities ($D\lambda^*$) of these stacked SiGe/Si 1111' detectors were estimated using the measure.ci quantum efficiency and dark current data. The detector with $p = 4 \times 10^{20}$ cm^{-3} shows

broad $D\lambda^*$ spectrum with $D\lambda^* > 1 \times 10^{10}$ cm$\sqrt{Hz}$/W at 40 K over 4-16 pm wavelength range; and detector with $p = 1 \times 10^{20}$ cm^{-3} shows $D\lambda^* > 1 \times 10^{10}$ cm$\sqrt{Hz}$/W at 60 K over 3-9 μm wavelength range.

5. ACKNOWLEDGMENT

'l'he work described in this paper was performed by the Center for Space Microelectronics Technology, Jet Propulsion Laboratory, California Inst it utc of Technology and was jointl y sponsored by the National Aeronautics and Space Administration, Office of Aeronautics, Exploration and "1'ethnology, the Ballistic Missile. Defense Organization, innovative Science and Technology Office, and the Air Force Rome Laboratory.

6. REFERENCES

1. T. L. Lin and J. Maserjian, *Appl. Phys. Lett.*, S7, 1422, (1990).

2.3'. L. Lin, A. Ksendzov, S. M. Dejewski, E. W. Jones, R. W. Fathauer, T. N. Krabach and J. Maserjian, *IEEE Trans. Electron Devices*, **38**, *1141*, (1991).

3. T. 1..1 in, T. George. E. W. Jones A. Ksendzov and M. 1.. 1 luberman, *Appl. Phys. Lett.*, 60, 380, (1992).

4. B-Y. Tsaur, C. K. Chen and S. A. Marine, *IEEE Electron Device Lett.*, 12, 293 (1 991).

5, B-Y. Tsaur, C. K. Chen and S. A. Marine, *SPIE Proceedings*, **vol.1540**, 580, (1991).

6. F. D. Shepherd, V. E. Vickers and A. C. Yang, "Schottk y-Barrier Photodiode with a I)egenerate Semiconductor Active Region," U.S. Patent No. 3603847, September 7, (197 1).

7. R. People, *IEEE J. Quantum Electronics*, **QE-22**, 1696, (1986).

8. T. L. Lin, J. S. Park, S. Gunapara, E. W. Jones and H. M. Del Castillo, submitted to *Optical Engineering*.

9. J. C. Bean, 1.. C. Feldman, A. '1'. Fiory, S. Nakahara and 1. K. Robinson, *J.* Vat. *Sci. Technol.*, A2, 436, (1984).

lo. T. 1.. Lin, R. W, Fathauer, P. J. Grunthaner, *Appl. Phys. Letts.*, *SS*, 795, (1989).

11. J. S. Park, R. P. G. Karunasiri, K. L. Wang, Y, J. Mii and J. Murray, *Material A!c.search Society Proceedings*, **vol.220**, 85, (1991).

12. P. J. Grunthaner, F. J. Grunthaner, R. W. Fathauer, 'l'. L. Lin, M. H. Hecht, L. D. Bell, W. J. Kaiser, 1:.11. Schowengerdt, and J. H. Mazur, *Thin Solid Films*, *183*, 197 (1989).

13. T. L. I in, E.W. Jones, T. George, A. Ksendzov and M. 1.. Huberman, *SPIE Proceedings*, **vol.1540**,135, (1991).

14. J. S. Park, R. P'. G.Karunasiri and K. L. Wang, *Appl. Phys. Lett.*, **61**, 681 (1992).

15.13. F.Levine, A, Zussman, S. D. Gunapala, M. 'J". Asom, J. M. Kuo and W. S. Hobson, *J. of Appl. Phys.*, *')2, 4429,* (1 *992).*

FIGURE CAPTIONS

Fig. 1. (a) Schematic cross section of a SiGe/Si HIP detector. (b) Energy band diagram of the SiGe/Si HIP detector and schematical illustration of detection mechanism.

Fig. 2. Energy band diagram of a stacked SiGe/Si HIP structure showing the detection mechanism.

Fig. 3. (a) Cross-sectional TEM micrographs of undoped, (b) HBO_2 boron doped $Si_{0.7}Ge_{0.3}$ layers grown by MBE at 5(IO °C.

Fig. 4. A SIMS profile of a typical elemental boron doped Si layers grown by MBE. It reveals 10 periods of p^+-Si layers with hyper sharp doping profiles. Delay length is about 20A.

Fig. 5. Cross-sectional TEM micrographs of a MBE grown multiple p^+-SiGe/p^--Si layer structure. The growth temperature was 380 °C and the c]c.mental boron was used for the growth of p^+-SiGe layers with 4x 102°" cm^{-3} doping concentrat ion.

Fig. 6. FTIR absorption spectra of multiple SiGe/Si layers with four periods of 50 Å p^+-$Si_{0.7}Ge_{0.3}$ /300 Å undoped Si layers. Boron doping is about $4 \times 10^{20} cm^{-3}$. It exhibits strong free carrier absorption.

Fig. 7. External quantum efficiency vs. wavelength for a stacked SiGe/Si HIP detector. The detector A consists of three 50 Å-thick p^+-$Si_{0.7}Ge_{0.3}$ layers which are separated by 300 Å-thick undoped Si layers. The boron concentration for the detectors is about 4 x 102°" cm^{-3}.

Fig. 8. The bias dependent photoresponse of detector A. The wavelength was fixed at 10 pm.

Fig. 9. The reverse bias current-voltage (J-V) characteristics of a stacked SiGe/Si stacked I 11P detector with four 25 Å p^+-$Si_{0.7}Ge_{0.3}$ layers separated by 300 Å undoped Si layers.

Fig.10. The activation energy plots for the stacked HIP detector shown in Fig. 9 at -0.1 V bias.

Fig. 11. External quantum efficiency vs. wave.length for stacked SiGe/Si 111P detectors with lower doping concentration. Detector C and D consist of three 50 Å-thick p^+-$Si_{0.7}Ge_{0.3}$ layers which are separated by 300 Å-thick undoped Si layers. Doping concentrations are about 1 x 10^{20} and 2 x 10^{20} cm^{-3} for detector C and D, respectivel y.

Fig. 12. The reverse bias J-V characteristics of detector D.

Fig.13. The estimated detectvity ($D\lambda^*$) vs wavelength at several temperatures for detector B and D.

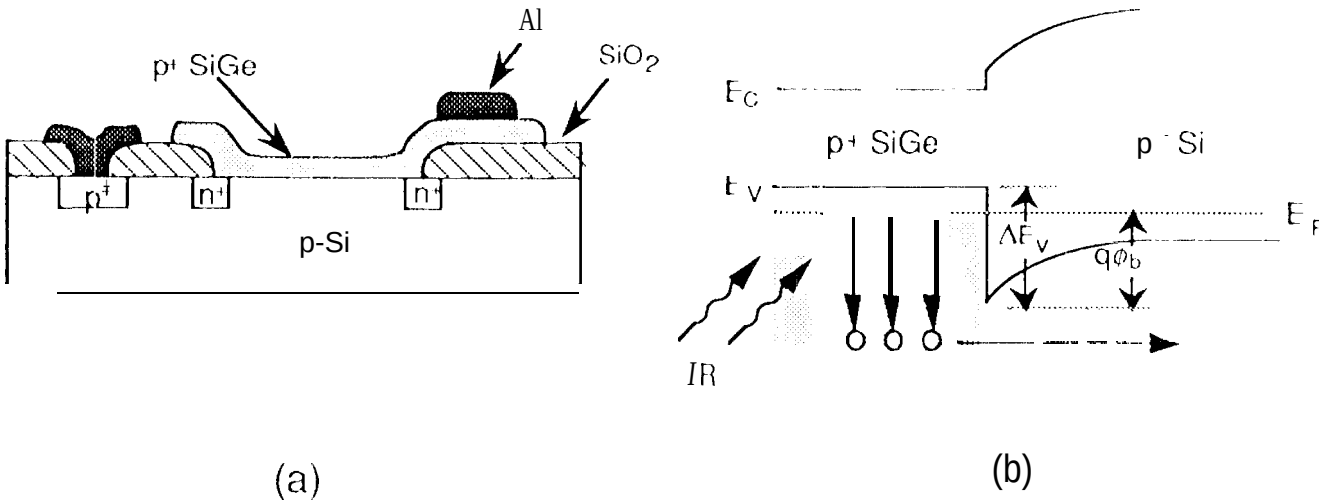
Al
SiO2
p+ SiGe
p+
n+
n+
p-Si
EC
p+ SiGe
p - Si
EV
EF
ΔEV
qφb
IR
(a)
(b)

Fig. 1

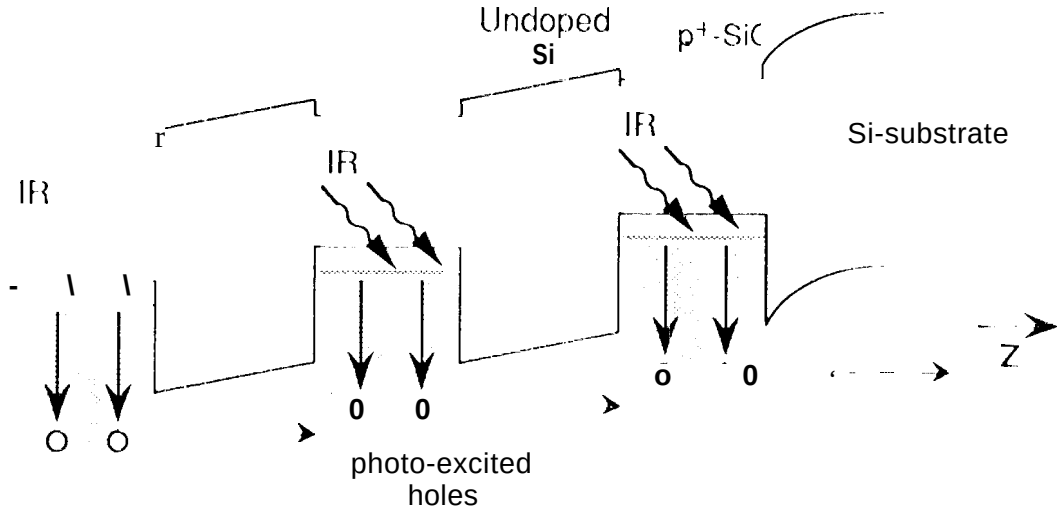
Undoped
Si
p+-SiC
Si-substrate
IR
IR
IR
0
0
0
0
photo-excited
holes
Z

Fig. 2

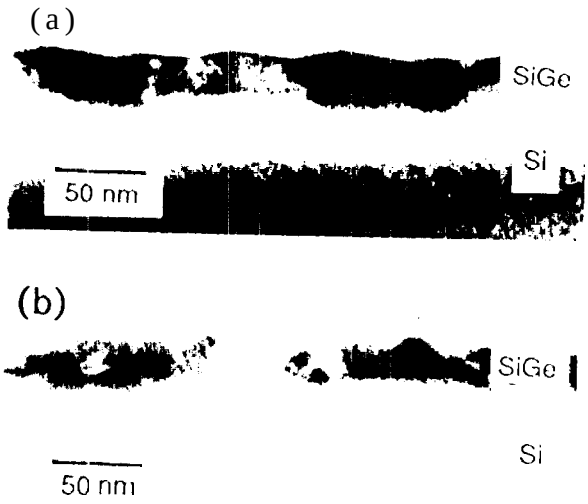
(a)
SiGe
Si
50 nm
(b)
SiGe
Si
50 nm

Fig. 3

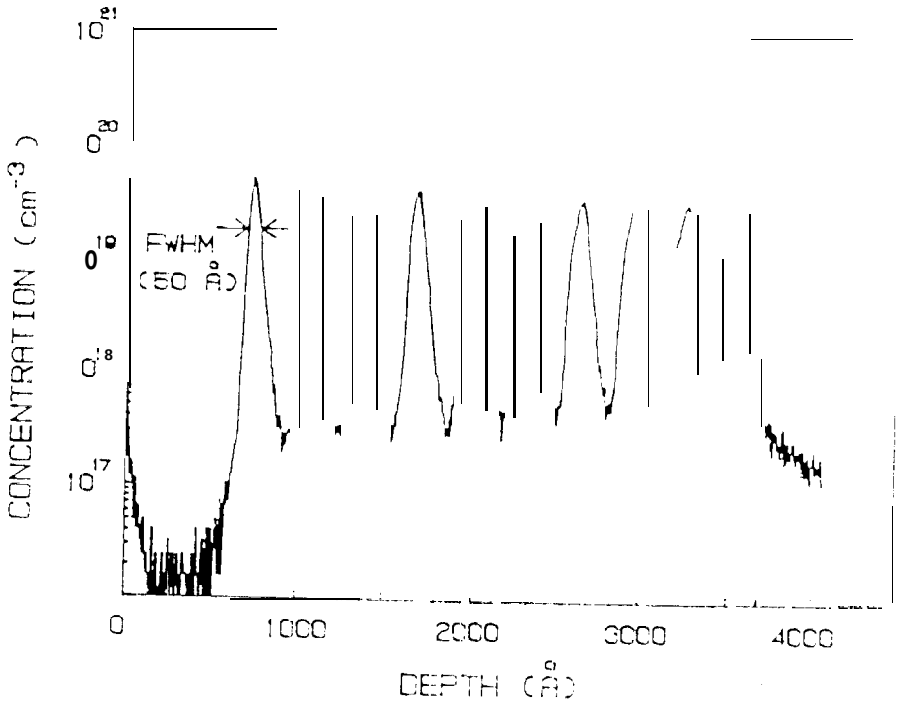
CONCENTRATION (cm-3)
FWHM
(50 Å)
0
1000
2000
3000
4000
DEPTH (Å)

Fig. 4

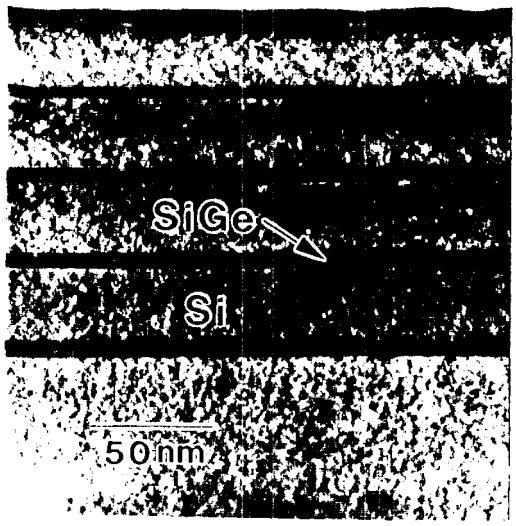
SiGe
Si
50nm

Fig. 5

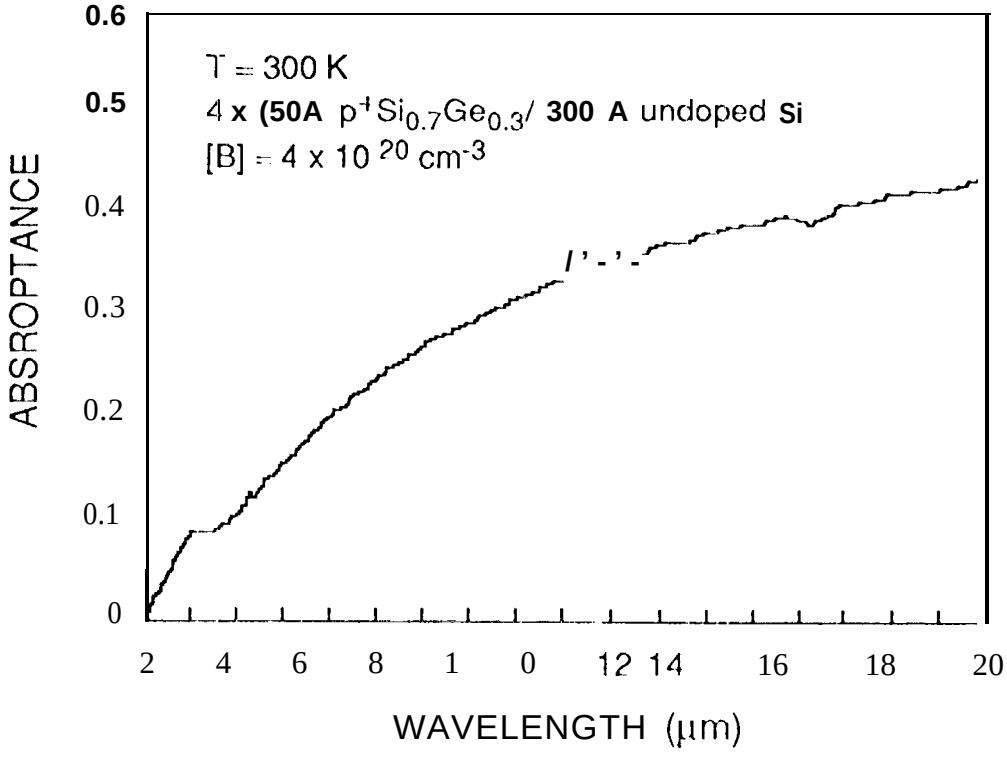
T = 300 K
4 x (50A p+Si0.7Ge0.3/ 300 A undoped Si
[B] = 4 x 10 20 cm-3
ABSROPTANCE
0.6
0.5
0.4
0.3
0.2
0.1
0
2
4
6
8
1
0
12
14
16
18
20
WAVELENGTH (μm)

Fig. 6

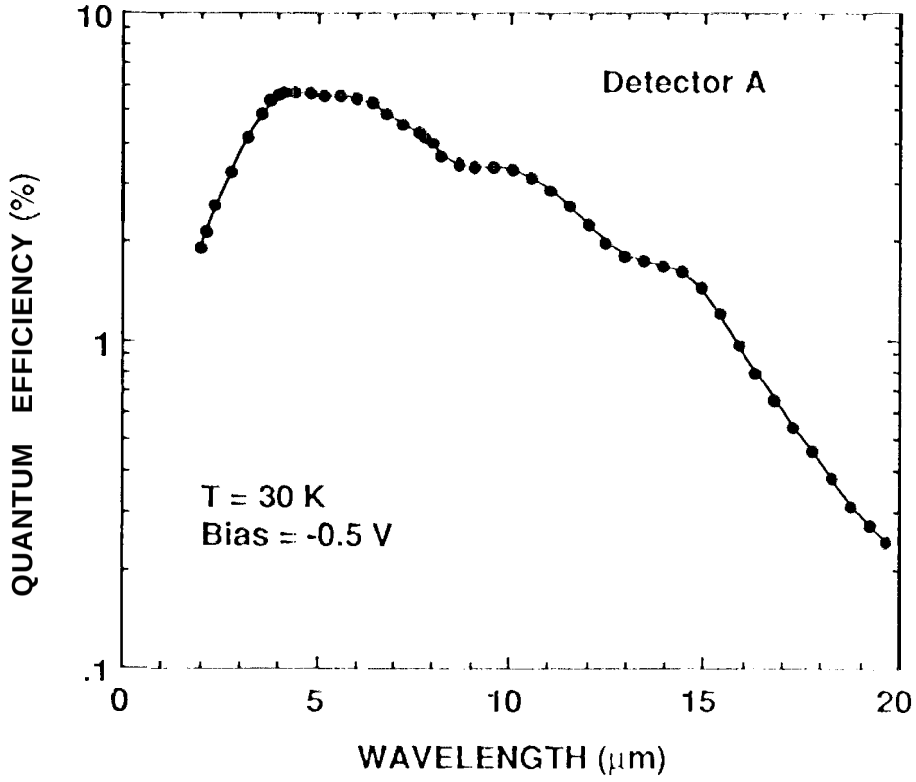
Detector A
T = 30 K
Bias = -0.5 V
QUANTUM EFFICIENCY (%)
10
1
.1
0
5
10
15
20
WAVELENGTH (μm)

Fig. 7

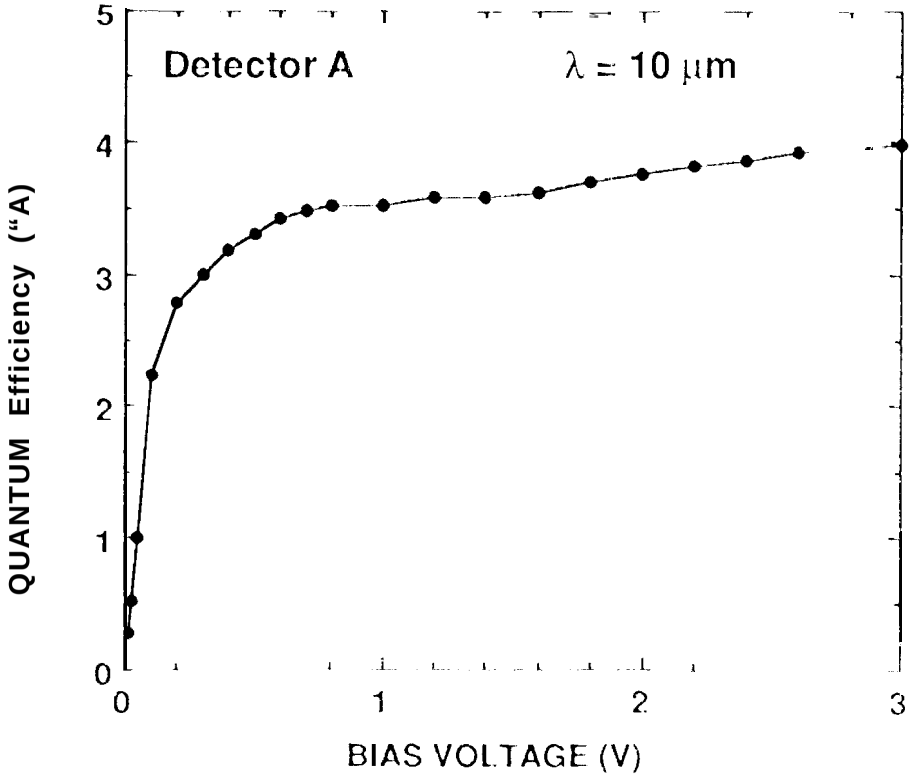
Detector A
λ = 10 μm
QUANTUM Efficiency ("A)
5
4
3
2
1
0
0
1
2
3
BIAS VOLTAGE (V)

Fig. 8

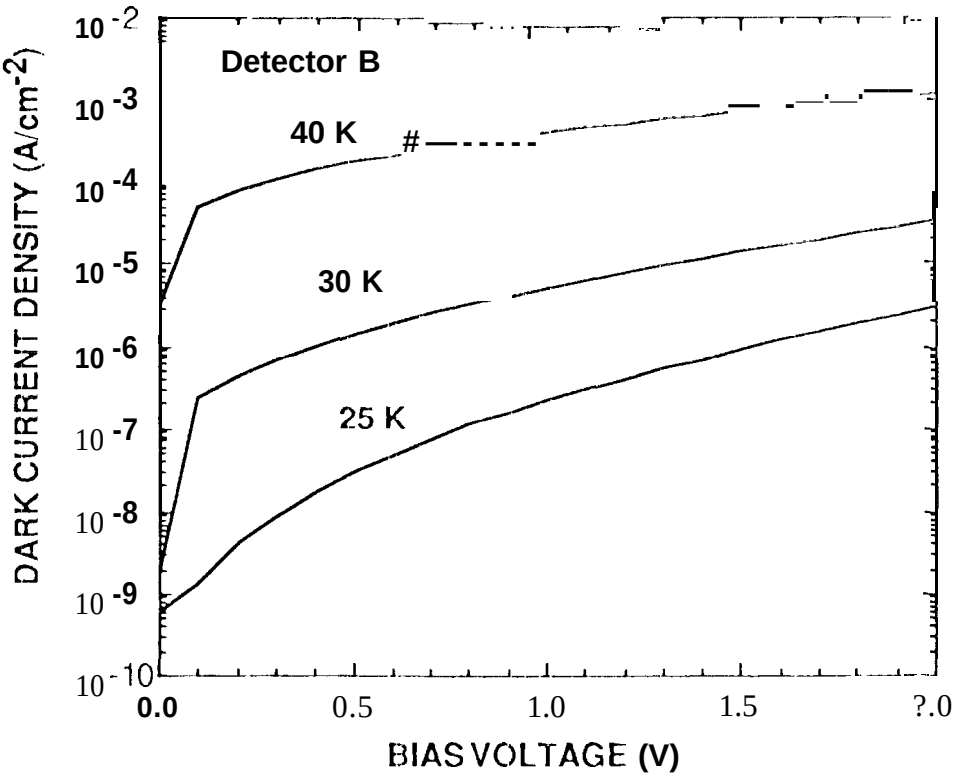
Detector B
40 K
30 K
25 K
DARK CURRENT DENSITY (A/cm-2)
10 -2
10 -3
10 -4
10 -5
10 -6
10 -7
10 -8
10 -9
10 -10
0.0
0.5
1.0
1.5
?.0
BIAS VOLTAGE (V)

Fig. 9

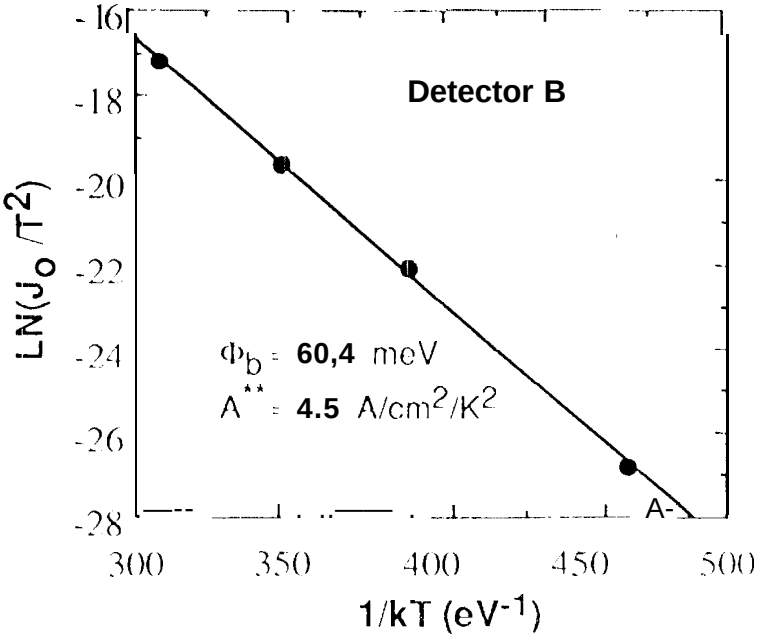
Detector B
Φb = 60,4 meV
A** = 4.5 A/cm2/K2
LN(Jo /T2)
-16
-18
-20
-22
-24
-26
-28
300
350
400
450
500
1/kT (eV-1)

fig. 10

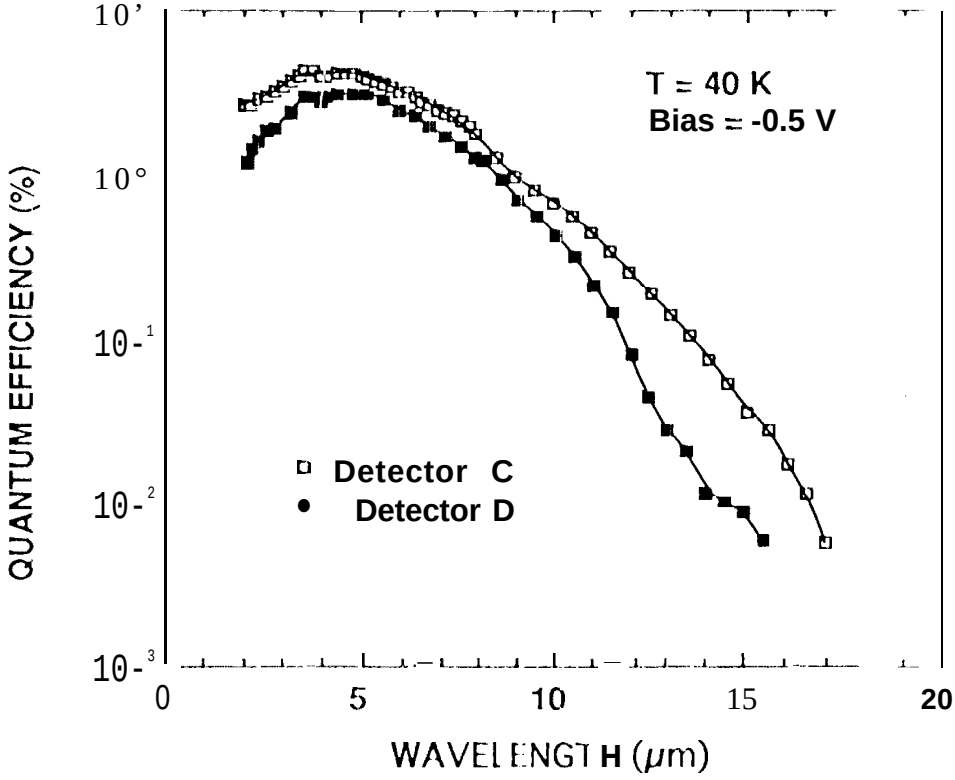
T = 40 K
Bias = -0.5 V
Detector C
Detector D
QUANTUM EFFICIENCY (%)
WAVELENGTH (μm)

Fig. 11

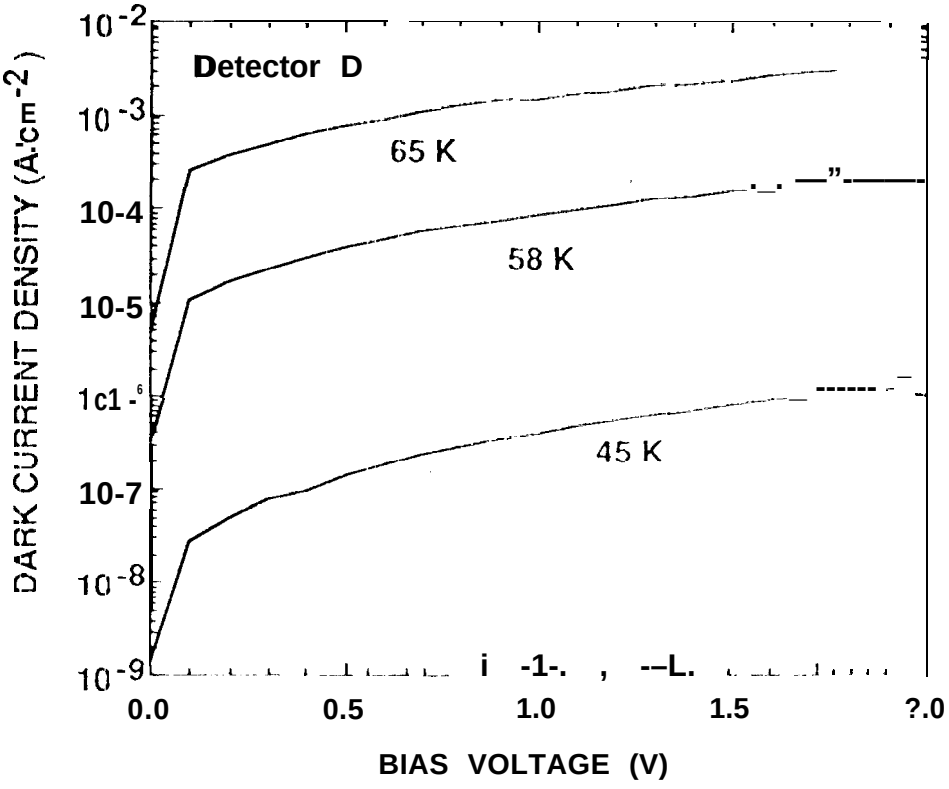
Detector D
65 K
58 K
45 K
DARK CURRENT DENSITY (A/cm-2)
BIAS VOLTAGE (V)

Fig. 12

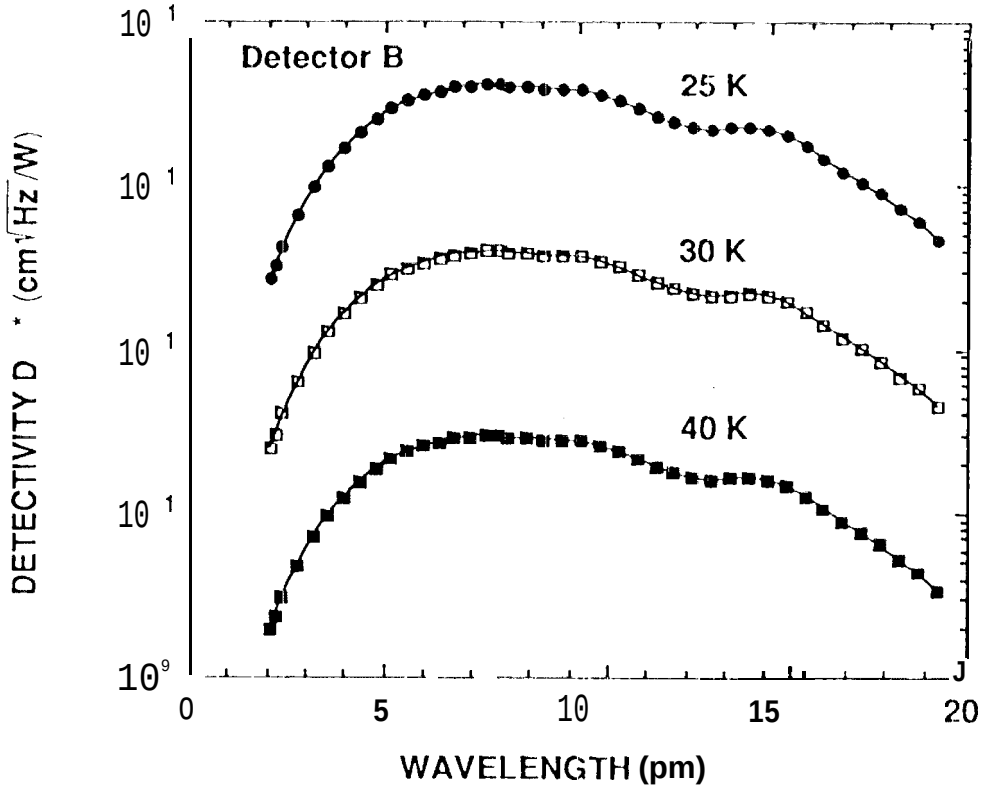
Detector B
25 K
30 K
40 K
DETECTIVITY D * (cm√Hz/W)
WAVELENGTH (pm)

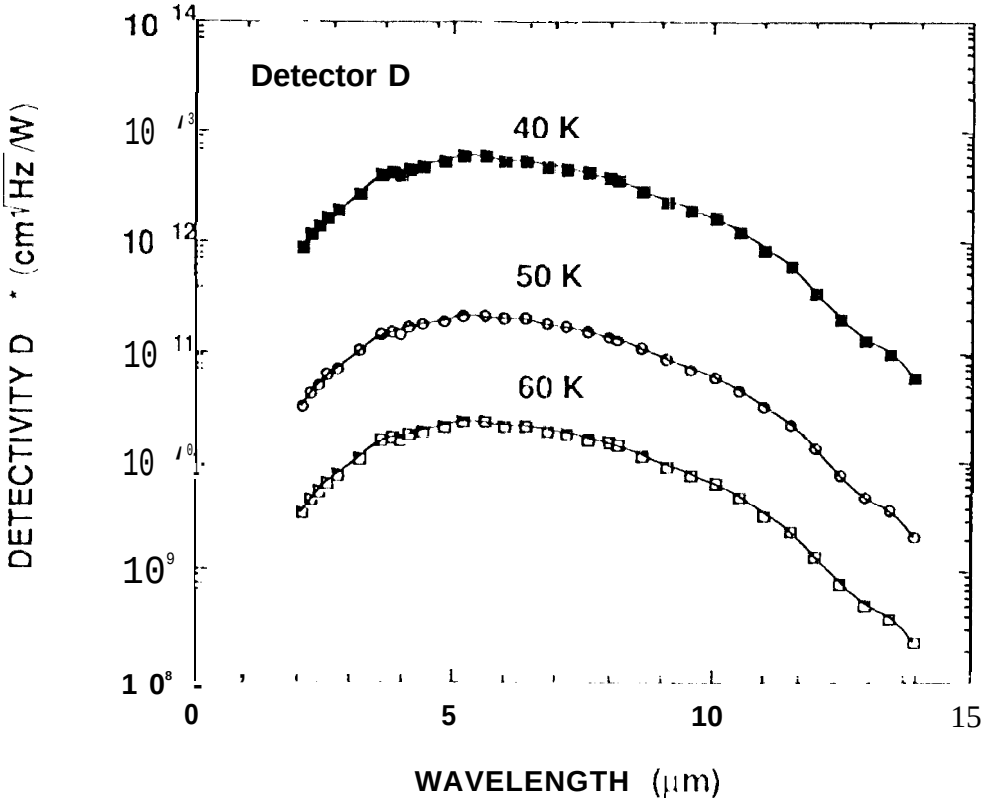
Detector D
40 K
50 K
60 K
DETECTIVITY D * (cm√Hz/W)
WAVELENGTH (μm)

Fig.13